Original Paper

Texture development of mesophase in reservoir pyrobitumen and the temperature-pressure converting of the gas reservoir in the Chuanzhong Uplift, Southwestern China

Cheng-Yu Yang [a], Mei-Jun Li [a, *], Tie-Guan Wang [a], Ning-Ning Zhong [a], Rong-Hui Fang [b, c], Long Wen [d]

[a] State Key Laboratory of Petroleum Resources and Prospecting, China University of Petroleum, Beijing, 102249, China
[b] Oil & Gas Survey, China Geological Survey, Beijing, 100083, China
[c] The Key Laboratory of Unconventional Petroleum Geology, China Geological Survey, Beijing, 100083, China
[d] Exploration and Development Research Institute of Southwest Oil & Gasfield Company, PetroChina, Chengdu, Sichuan, 610041, China

A R T I C L E   I N F O

A B S T R A C T

The Neoproterozoic-Lower Paleozoic dolostone gas reservoirs in the Chuanzhong Uplift in Southwestern China contain the mesophase pyrobitumen (pyrobitumen with mesophase). The mesophase in the pyrobitumen is mostly composed of a mixture of condensed macromolecule polycyclic aromatic hydrocarbons (PAH), and has been mostly converted to various grain, flow, and domain textures. The volcanic activity nearby the Chuanzhong Uplift may have generated very hot (over 300 °C) hydrothermal fluid, with migration of the fluid into the dolostone reservoir transforming the hydrocarbons in the reservoir into an anisotropic carbon by-product, which formed under high temperature and pressure conditions; over 300 °C and 200 MPa according to fluid inclusion analysis. The high temperature-pressure in reservoir was caused by sudden devolatilization of the hydrocarbons due to hydrothermal heating, which formed the unusual texture of the mesophase. The elliptical mesophase grains (EG), the honeycomb structure of pyrobitumen, and the occurrence of polarized classes of mesophase in single pyrobitumen deposits are all unusual textures. This study investigates the texture development of this pressure-affected pyrobitumen. Observation and study of the mesophase suggest that the class of mesophase in pyrobitumen is determined by temperature, while pressure (assessed from associated fluid inclusions) significantly affected the texture. Analysis of the texture of the pyrobitumen in conjunction with previous thermometry results from methane inclusions suggests that the high class mesophase of the pyrobitumen could be applied as a temperature indicator for geological conditions. Furthermore, the unusual textures of the pyrobitumen including elliptical mesophase grains (EG), the honeycomb structure of pyrobitumen, and the occurrence of polarized classes of mesophase in single pyrobitumen could reflect the abnormal high formation pressure.

1. Introduction

Experiments have found that petroleum and coal pitches are transformed to mesophase at fairly high temperatures (350−500 °C) (Marsh, 1973; White, 1976; Forrest and Marsh, 1981; Mochida et al., 1984; Goodarzi, 1984, 1985; Goodarzi and Stasiuk, 1991). Mesophase is a common carbon material precursor that is composed of a mixture of condensed macromolecule polycyclic aromatic hydrocarbons (PAH) produced by disproportionation reactions, including pyrolysis and polycondensation (White, 1976; Lewis, 1978, 1980, 1987; Klett et al., 2000). Mesophase is the liquid crystal of graphitized organic matter, first discovered by Brooks and Taylor and characterized, based on its microtexture, using optical microscopy (OM) and scanning electron microscopy (SEM) (Brooks and Taylor, 1965). Thermal treatment of petroleum and coal pitches at temperatures of > 350 °C results in the formation of spherical mesophase (liquid crystal) in an isotropic matrix (Brooks and Taylor, 1965; White, 1976; Lewis and Kovac, 1978; Forrest and Marsh, 1981). Increasing temperature eventually results in

coalescence of the mesophase spheres, finally forming domain mesophase after passing through a flow mesophase stage (Ragan and Marsh, 1981).

Geologically, mesophase commonly occurs in pyrobitumen as the solid product of petroleum cracking in reservoirs and overmature source rocks (Jacob, 1989; Rippen et al., 2013; Emmanuel et al., 2016; Hackley and Cardott, 2016; Mastalerz et al., 2018). The generation of mesophase under geological conditions has always been observed in association with high pressure, which may be due to pressure exerted by overlying strata or a phase change in the formation fluids (Barker, 1990; Svensen et al., 2009; Yang et al., 2018a, 2018b). The development of mesophase texture is therefore controlled by both temperature and pressure (Goodarzi, 1985; Santamaria et al., 1999). This suggests that the optical characteristics of pyrobitumen might provide a record of the geological temperature/pressure conditions associated with its formation in reservoirs. Until now, pyrobitumen has not conventionally been used as a geological pressure indicator.

Previous studies have described mesophase in reservoirs in detail, with the microtextures appearing to differ from those in mesophase produced under experimental conditions (Yang et al., 2018a; Gao et al., 2018). Generation of mesophase in the reservoir of the Anyue Gas Field occurred under formation pressure (Yang et al., 2018a; Gao et al., 2018), with the cracking of the oil leading to a momentary high pressure surge in the pore system (Zou et al., 2014; Zhu et al., 2015; Yang et al., 2018b). In this study, optical and morphological investigation of the texture of the reservoir pyrobitumen is carried out, based on understandings gained in previous studies, and the influence of high pressure conditions is explored.

2. Geologic setting

2.1. Location and stratigraphy of the gas field

Mesophase has been discovered in the dolostone reservoirs of the Weiyuan and Anyue Gas Fields in the Chuanzhong Uplift in the central Sichuan Basin (Fig. 1a and b). Previous studies have shown that this gas field was once a large oil field, and that *in-situ* coking converted the liquid oil into gas and pyrobitumen (Wei et al., 2013; Zou et al., 2014; Zhu et al., 2015). This pyrobitumen contains mesophase, and natural gases fill the vugs, pores, and cracks in the dolostone (Wei et al., 2013; Zou et al., 2014; Zhu et al., 2015; Yang et al., 2018a). The vugs, pores, and cracks in the dolostone are generally well connected due to a previous karstification event. The stratigraphy of the gas field includes, from bottom to top, the Ediacaran Doushantuo (Z_1ds) and Dengying Formations (Z_2dn1-4),

and the Early Cambrian Qiongzhusi ($\in_1q$), Canglangpu ($\in_1c$), and Longwangmiao formations ($\in_1l$) (Wei et al., 2013; Zou et al., 2014). However, the upper Cambrian formations are mostly absent in the southwest part of the Weiyuan Gas Field (Fig. 1a). The petroleum system is composed of Ediacaran-Cambrian carbonate successions, which include the source rocks in the Z_1ds, Z_2dn3, and $\in_1q$ formations and the dolostone reservoir rocks of the Z_2dn2, Z_2dn4, and $\in_1l$ formations (Wei et al., 2013; Zou et al., 2014). The Lower Cambrian $\in_1q$ Formation is drilled by wells Gs17 and is the principal source rock for the currently identified gas reservoirs. The kerogen type is I to II of the $\in_1q$ Formation source rock which lies in a sag between the reservoirs of Anyue Gas Field and Weiyuan Gas Field (Wei et al., 2013; Zou et al., 2014; Zhu et al., 2015; Yang et al., 2018a). The oil from the source rock accumulated in the nearby reservoirs (Wei et al., 2013; Zou et al., 2014; Zhu et al., 2015). Other potential source rocks in Z_1ds and Z_2dn3 have not yet been identified. The three reservoir sections (the Z_2dn2, Z_2dn4, and $\in_1l$ formations) are divided by the Z_2dn3 and $\in_1q$ formations, which are composed of low permeability shale (Zou et al., 2014; Liu et al., 2018; Yang et al., 2018a, 2018b). However, faults connect the reservoirs, serving as pathways for oil migration and creating a unified petroleum system (Zou et al., 2014; Liu et al., 2018; Yang et al., 2018a, 2018b). Mesophase has been found in the Z_2dn2, Z_2dn4, and $\in_1l$ formations throughout the Chuanzhong Uplift (Yang et al., 2018a; Gao et al., 2018). Gas has accumulated in the Weiyuan Gas Field and the Anyue Gas Field (Fig. 1a and b) (Zou et al., 2014; Zhu et al., 2015).

2.2. The emeishan large igneous province

A magmatic plume of predominantly basaltic composition occurred during the late Permian. This plume is commonly known as the Emeishan large igneous province (ELIP), or Emeishan traps. It intruded into the southwestern part of the South China Plate (Fig. 1a) (Chung and Jahn, 1995). The ELIP covers an area of at least 2.5×10^5 km^2 in the western margin of the Sichuan Basin and is also likely to be present, but concealed, in the central part of the basin (He et al., 2003). It was a major thermal event affecting the entire Sichuan Basin, featuring magmatic activity and causing hydrothermal mineralization across the basin (Jiang et al., 2016; Liu et al., 2016, 2018; Yang et al., 2018b). Migration of hydrothermal fluid within the Ediacaran-Cambrian carbonate successions during the event is considered to be the cause of the oil coking that generated pyrobitumen in the reservoir (Yang et al., 2018a, 2018b). Evidence of hydrothermal mineralization is common in cores drilled in the Chuanzhong Uplift. These minerals include sphalerite and galena;
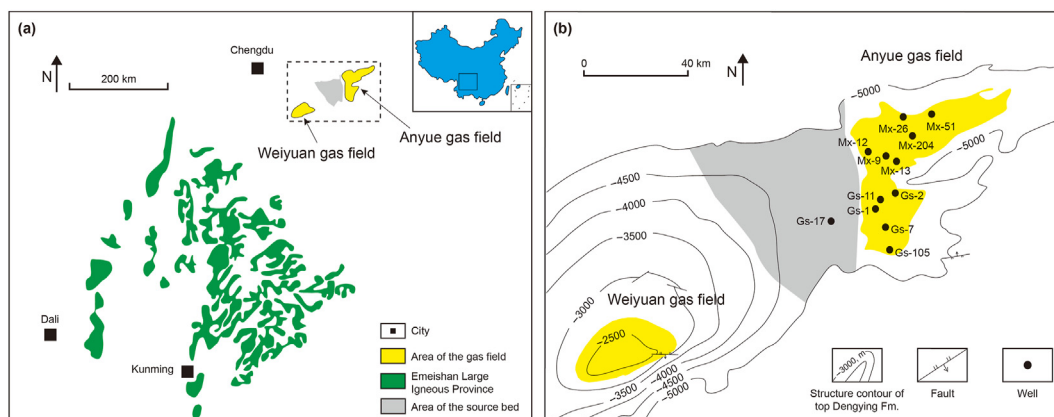

Fig. 1. Map of the Geological settings in Chuanzhong Uplift (**a**), the location of cored wells in the Chuanzhong Uplift (**b**) is the dotted box in map (a).

i.e., the typical assemblage in a lead-zinc vein (Jiang et al., 2016; Liu et al., 2016; Yang et al., 2018b). Analysis of methane inclusions in the hydrothermal minerals has revealed that the formation temperature of these minerals was likely to have been > 300 °C (Yang et al., 2018b). Previous studies have concluded that the ELIP triggered a hydrothermal event that caused hydrothermal fluids to migrate from the southwest to the northeast of the Chuanzhong Uplift (Jiang et al., 2016; Liu et al., 2016, 2018; Yang et al., 2018b).

3. Samples and methods

3.1. Samples

Reservoir pyrobitumen samples (pyrobitumen within rock) from the Z_2dn2, Z_2dn4, and $\in_1 l$ formations were collected from exploration wells within a depth range of 4573−5517 m (Yang et al., 2018a). Pure pyrobitumen was concentrated from the dolostone for enhanced observation using scanning electron microscopy (SEM) and element determination. Half of the bituminous core samples were crushed into small pieces, with diameters of 1−2 cm, and immersed in 3 mol/L hydrochloric acid at 35 °C for 10 h to remove carbonates. These relatively large pyrobitumen clastics were then selected for SEM observation. The rest of the samples were pulverized to below 200 mesh and once again reacted with 3 mol/L hydrochloric acid at 35 °C for 10 h to remove carbonates for elemental analysis. Immersion in hydrofluoric acid (40% mass fraction) at 25 °C for 5 h was then used to remove silicates.

3.2. Microscopy and elemental analysis

The samples were polished using the standard method (Stach et al., 1982; Kilby, 1988; Luo et al., 2014) and examined under a Leica DM4500P microscope with an oil-immersion objective, using reflected light (Goodarzi and Stasiuk, 1991; Yang et al., 2018a). Bitumen reflectance under oil immersion (%BR$_o$) was measured at a wavelength of 546 nm (1.518 refractive index oil) using a CRAIC Microscope photometer. The measurements were calibrated against standards of known reflectance (Cubic-Zirkonia, R_o = 3.08% and Strontium Titanate, R_o = 5.39%) (Luo et al., 2014, 2016, 2017). The measurement spot size was 1 μm^2 and 30−50 points were measured on each sample. Both the maximum (%BR$_{omax}$) and minimum (%BR$_{omin}$) reflectance values of the bitumen were measured with rotation under the oil objective using polarized light (Stach et al., 1982; Kilby, 1988).

SEM was used to observe the morphology of the pyrobitumen. The large clastic dolostone samples containing pyrobitumen and pure pyrobitumen were coated with gold and analyzed using a Hitachi SU8010 and a ZEISS MERLIN compact field emission SEM. The samples were fixed on a metal plate using conductive adhesive and covered with gold, and the plates left to settle in the sample room for observation.

Element analysis of the pure pyrobitumen was performed on an Elementar Vario EL CUBE analyzer. The acidified powder from each of the samples was used in the element analysis and the weights (wt%) of C, H, and reported by the analyzer. The H/C atomic ratios were then calculated from the molecular weights of C and H.

4. Results

4.1. Classification of the pyrobitumen

Following experimental and chemical study of the mesophase, a classification was determined consisting of 8 classes according to the shape and size of the mesophase (White, 1976; Lewis, 1978,1980,1987; Ragan and Marsh, 1981; Klett et al., 2000). The increasing size of the mesophase is due to increase size and number of PAH with increasing temperature (White, 1976; Lewis, 1978, 1980, 1987). The mesophase is usually all grain at first, with the grain subsequently coalescing to form flow and domain mesophase (Table 1) (Ragan and Marsh, 1981). The full range of mesophase, as set out in the classification by Ragan and Marsh (1981), occurs in the reservoir pyrobitumen in the Chuanzhong Uplift (Fig. 2). The concept and terminology of this previous classification of mesophase is therefore followed (Goodarzi, 1985; Stasiuk, 1997; Santamaria et al., 1999). The classification of Ragan and Marsh (1981) mainly based on the statistic of optical size and shape evolution of the mesophase, but the classification scheme for pyrobitumen has not been discussed in previous literature.

The grained-mozaic mesophase is mostly elliptical in the reservoir pyrobitumen in Chuanzhong Uplift and commonly displays a framework construction (Fig. 2a). Although the grain mesophase always has an anisotropic texture (Brooks and Taylor, 1965; White, 1976; Ragan and Marsh, 1981), randomly arranged Mf manifests as isotropic texture in matrix (Fig. 2b). Oppositely, the anisotropic texture of the Mm and larger mesophase can be displayed in the microphotographs (Fig. 2c−f). The stacks of PAH lamellae observed on the SEM images reveal the inner texture of different classes of mesophase. The PAH lamellae in the assemblage of Mf and Mm are short and slightly curved, and distributed in an inconsecutively and fairly compact arrangement (Fig. 2d), while the CF and FD shows an oriented extinction controlled by the trend of the PAH lamellae in the CF and FD (Fig. 2d,−f). Generally, flow and domain mesophase are composed of lamellae that are larger, straighter, and more compact (Fig. 2d, g, h, i). As shown in the images, the PAH lamellae in the domain mesophase are straightly extended (Fig. 2g), but have been overturned by folding (Fig. 2i). Folding of PAH lamellae is common in domain mesophase, since this type of mesophase must remain in the liquid phase while it is forming (White, 1976). Coking of pitch (oil under geological conditions) volatilizes the gases which would otherwise exert external force on the PAH lamellae (White, 1976). The effect of this external force is insignificant in grain mesophase because the grains are separated. However, in domain mesophase, the force compresses the PAH lamellae to form folds (Fig. 2i).

To simplify the terminology for the reservoir pyrobitumen, it is classed as one of the three types: matrix pyrobitumen (MP), grain pyrobitumen (GP), or domain pyrobitumen (DP) (Table 1). MP consists entirely of Mf mesophase (Fig. 2b). Different classes of grain-mozaic mesophase commonly occur with flow and domain mesophase in GP (Fig. 2c, e, f). DP is composed only of domain mesophase (Fig. 2h).

4.2. Unusual textures of mesophase in pyrobitumen

4.2.1. Elliptical grain (EG)

Mesophase grain in laboratory experiments is usually spherical, with the grain in the higher classes of mesophase commonly becoming enlarged before they coalesce to form flow texture (Brooks and Taylor, 1965; White, 1976; Ragan and Marsh, 1981). However, spherical mesophase grain is not found in reservoir pyrobitumen of Chuanzhong Uplift; all of the grains are elliptical (Fig. 3).

Mf in the reservoir pyrobitumen is usually randomly arranged, appearing as a framework in MP and coating the coarser Mf and Mm in GP (Fig. 3a−c). However, several oriented Mf can be observed in the MP (Fig. 3b). Lamellae are observed on the cross-section of the long axis of the elliptical grain (Fig. 3d). These are condensed macromolecule PAH lamellae, which are the basic constituents of mesophase (Lewis and Kovac, 1978; Lewis, 1980, 1987; Greinke, 1990; Wang, 1990).

Table 1
The classification of mesophase in pyrobitumen (Ragan and Marsh, 1981, modified).

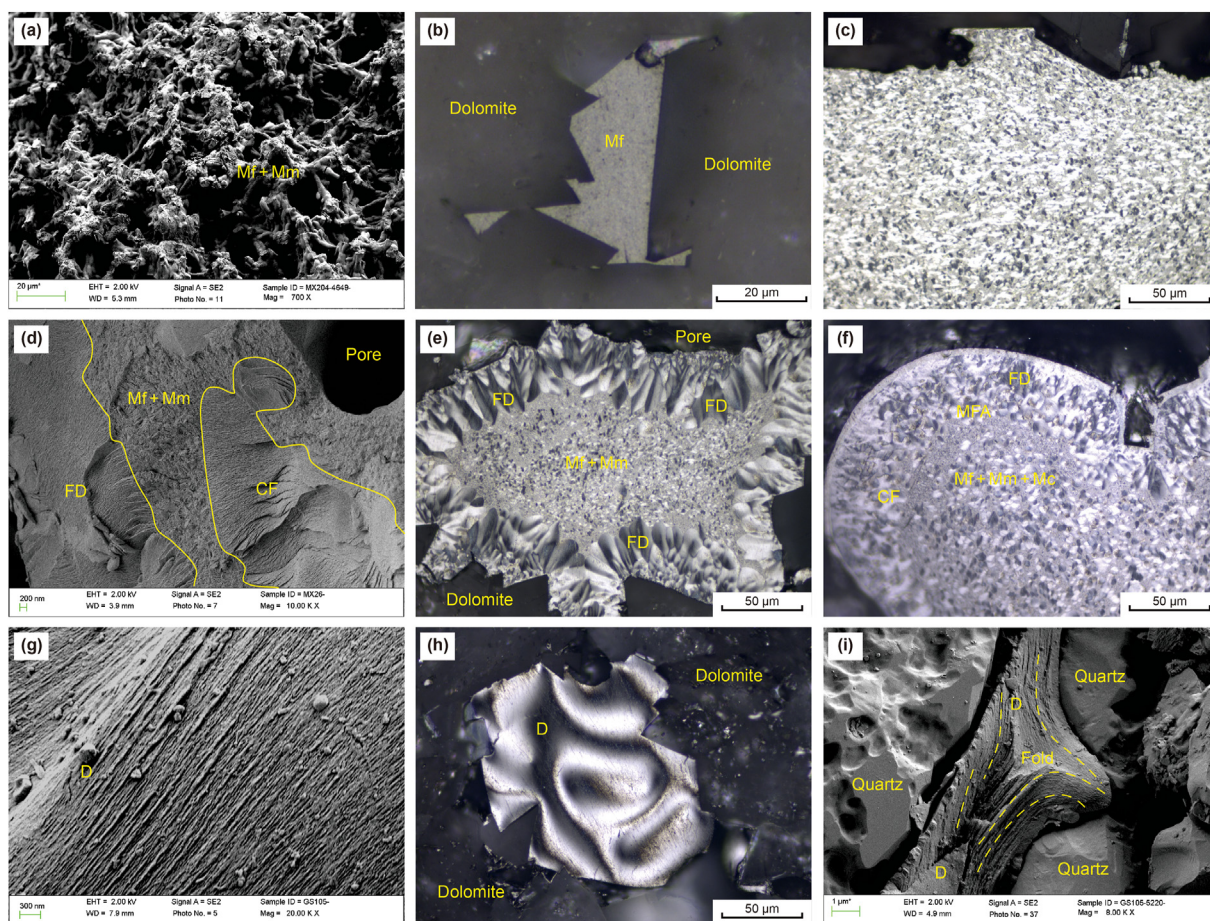| Hydrocarbon	Terminology	Code	Characteristics
Mesophase	Fine-grained mozaic	Mf	0.5–1.5 μm in diameter
	Medium- grained mozaic	Mm	1.5–5 μm in diameter
	Coarse- grained mozaic	Mc	5–10 μm in diameter
	Supra-mozaic	SM	Area of mosaic where carbon layer planes are orientated in a similar direction
	Medium-flow anisotropy	MFA	< 30 μm in length; < 5 μm in width
	Coarse-flow anisotropy	CF	< 60 > 30 μm in length; < 10 > 5 μm in width
	Flow domain anisotropy elongated	FD	> 60 μm in length; > 10 μm in width
	Domains	D	> 60 μm in diameter
Pyrobitumen	Matrix pyrobitumen	MP	Only composed by Mf (> 95%)
	Grain pyrobitumen	GP	Different classes of mesophase
	Domain pyrobitumen	DP	Only composed by D

Fig. 2. Texture of different classes of pyrobitumen under SEM and polarized reflect light. (**a**): the mesophase grains of framework construction, Mx-204-4649 m. (**b**): the MP only contains Mf, Gs-11-4673 m; (**c**): the mesophase grains (Mf + Mm + Mc) of framework construction, Mx-12-4659 m; (**d**): GP contains multiple classes of mesophase, the PAH lamellas in the area of Mf + Mm are mixed, while they are better ordered in the area of CF and FD, Mx-9-5033 m; (**e**): GP contains multiple classes of mesophase, Mx-9-5033 m; (**f**): GP contains multiple classes of mesophase, Mx-204-4681 m; (**g**): PAH lamellas in domain mesophase is well sustained and compressed, Gs-105-5220 m; (**h**): domain mesophase only contains domain mesophase, Gs-7-5328 m; (**i**): the fold of the compressed PAH lamellas in the domain mesophase (SEM), Gs-105-5220 m.

4.2.2. Orientation of EG

Oriented EG groups are the SM in the experimental mesophase (Table 1) (Ragan and Marsh, 1981). The formation of SM is easier in the reservoir pyrobitumen for the elliptical shape of the grained-mozaic which is observed by the SEM (Fig. 3). SEM images show that the Mf tends to orient (Fig. 3a and b) in the reservoir pyrobitumen and confer an optically anisotropic texture on the MP (SM-Mf) (Fig. 4a and b). As can be seen from the optical images, groups of Mm are also oriented in a single direction (SM-Mm), but the direction of the oriented EG groups is random (Fig. 4c and d). The mass of

oriented grains are therefore uniformly extinguished under polarized light (Fig. 4a–d). However, the uniformly extinction is never observed on the isotropic Mf in the pyrobitumen (Fig. 4e and f).

4.2.3. Multiple classes of mesophase in GP

The texture of the mesophase in experimental samples is usually a single class in each individual pyrobitumen (White, 1976; Ragan and Marsh, 1981). However, multiple classes of mesophase commonly occur together in the GP (Fig. 2c, d, e, f). These multiple classes of mesophase in individual pyrobitumen deposits create a
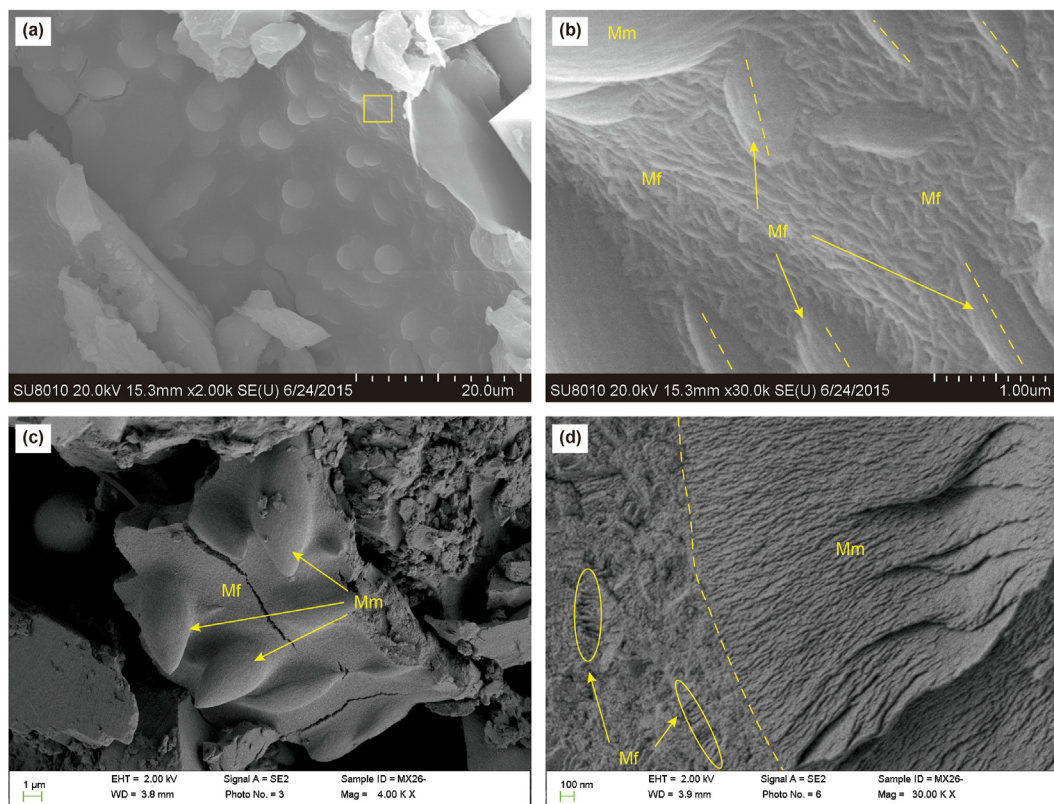
Fig. 3. Shape and texture of the EG mesophase in pyrobitumen under SEM. (**a**): the surface of a pyrobitumen in the pore of the reservoir rock, the humps are the Mms, Mx-13-5104 m; (**b**): the close-up of pyrobitumen shows the EG (yellow square in Fig. 3a); the larger Mfs are oriented while the smaller Mfs are interlaced in the pyrobitumen, Mx-13-5104 m; (c): surface of the GP with Mfs and Mms, Mx-26-4910 m; (**d**): the Mfs and Mms in the pyrobitumen, the Mfs are within the isotropic matrix, composed by very short PAH lamella which is loosely arranged, whereas the Mm is composed by longer PAH lamellas with a "cleavage structure", Mx-26-4910 m.

special texture in the reservoir samples (Yang et al., 2018a). In the reservoir samples, the multiple classes of mesophase include groups of Mf or SM-Mf, coated on higher class mesophase grains (Mm, Mc) or even flow and domain mesophase (Fig. 2c—f) (Fig. 3b, d).

4.3. Distribution of the pyrobitumen in the reservoir

Pyrobitumen was discovered from Z_2dn2, Z_2dn4 and ϵ_1l formations in the Anyue Gas Field (Fig. 5). The gas reservoirs commonly occurred together with the pyrobitumen. Different class mesophases included in pyrobitumen are in fluctuating ratios (Fig. 2c—f).

Generally, the MP is only discovered from the top of the ϵ_1l formations which is also the top of all the gas reservoir, while the DP is only discovered at the bottom of the gas reservoir or nearby the top of Z_2dn4 which is the most significant plane of unconformity in the gas reservoirs (Table 2). GP is the most common pyrobitumen in the middle of the gas reservoir. However, the class of mesophase occurred in the GP is related to the formations. The raising mesophase class is observed in the GP in the ϵ_1l formation. That means the lowest class mesophase to the highest class mesophase is consecutive. However, in the deeper reservoir of Z_2dn2 and Z_2dn4 formations the medium class mesophase (Mc, MFA) frequently absent (polarized classes of mesophase in single pyrobitumen) (Table 2).

The %BR_{omax} of pyrobitumen is increasing with the depth of the samples. Meanwhile, the H/C atomic ratio of pyrobitumen is decreasing with the depth of the samples (Table 2). This transformation is agree with the texture evolution of the mesophase. Because the pyrobitumen in deeper reservoir have more high class

mesophase which have higher %BR_{omax} and lower H/C atomic ratio for its larger and more compressed PAH (Brooks and Taylor, 1965; White, 1976; Lewis and Kovac, 1978; Forrest and Marsh, 1981). SM-Mf groups are found in both MP and GP (Table 2). It is worth noting that, in the deeper reservoir, most of the pyrobitumen has turned to DP (Table 2). However, the SM-Mm did not coalesce, but maintained their size and appear as grain mesophase (Fig. 4c and d).

5. Discussion

5.1. What caused the thermal alteration of the hydrocarbons?

The ELIP triggered intrusion of hydrothermal fluid into the reservoir during the late Permian, coinciding with the greatest thermal event in the basin's geological history (Zhu et al., 2015; Yang et al., 2018b; Liu et al., 2018; Gao et al., 2018). Lead-zinc veins, which are common indicators of hydrothermal fluids (Large et al., 2002; Basuki and Spooner, 2004; Leach et al., 2005, 2010), have been discovered in the reservoir in the Chuanzhong Uplift. Ore veins are commonly created by hydrothermal fluid invasion, with a fluid inclusion thermometry range of 50—300 °C (Large et al., 2002; Basuki and Spooner, 2004). The hydrothermal fluid is formed during fluid migration, or is triggered by volcanic activity, which usually leads to higher temperatures in the fluids (Leach et al., 2005, 2010).

The pyrobitumens analyzed in this study were not formed under normal geological maturation conditions. Influenced by time, temperature, and pressure, they have been altered by the migration of high temperature hydrothermal fluid at over 300 °C into the reservoir (Yang et al., 2018b), which rapidly altered the
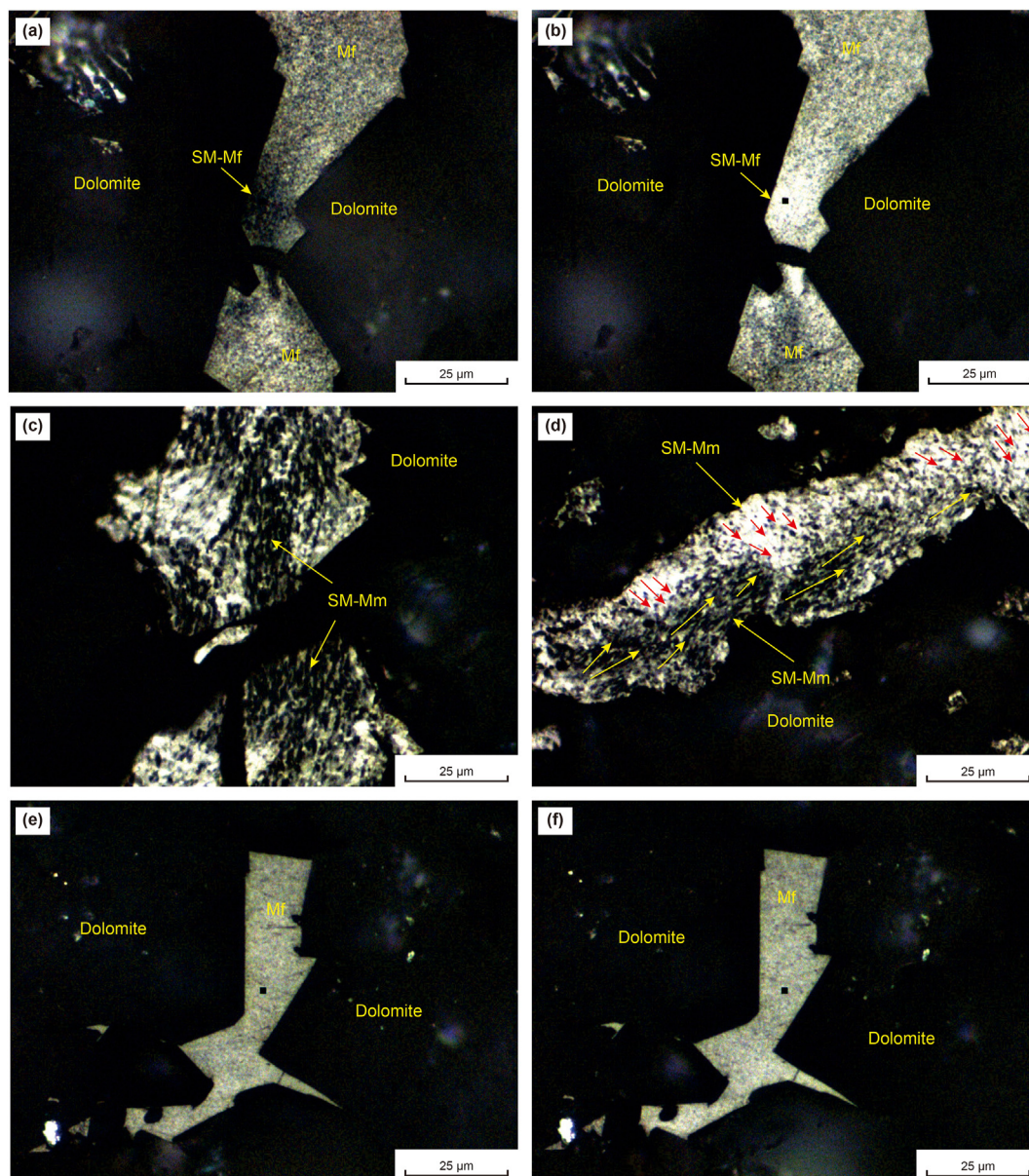
Fig. 4. Oriented texture of the EG in the pyrobitumen samples under polarized reflect light. (**a**): the SM-Mf have uniform extinction in MP, Gs-11-4673 m; (**b**): after the rotation of 45° the SM-Mf was brightened, Gs-11-4673 m; (**c**): SM-Mm have uniform extinction and pixel level domain structure, Mx-51-5395 m; (**d**): different orientation of the SM-Mm in the individual pyrobitumen, Mx-51-5395 m. (**e**): the isotropic Mf in MP, Gs-11-4673 m; (**f**): after the rotation of 45 degree of the isotropic Mf, Gs-11-4673 m.

hydrocarbons (Gentzis, and Goodarzi, 1993; Rimmer et al., 2015; Gao et al., 2018; Yang et al., 2018a). With increasing depth in the reservoir, the pyrobitumens display enhanced mesophase classes and increasing %BR_{omax} (3.32%−8.54%) (Table 2). However, the unusually low %BR_{omax} (2.49%) of the pyrobitumen in the source rocks (Gs-17 shale) indicates unequal temperature distribution (Table 2). It is likely that high volumes of hydrothermal fluids invaded the reservoir through the high-permeability pore system created by earlier karstification (Wei et al., 2013; Zou et al., 2014). However, the flow of hydrothermal fluid was impeded by the low permeability source rocks. It did not generate a burial thermal event sufficient to heat the rock formations themselves to a similar extent. Studies of the burial-thermal history of the Chuanzhong Uplift indicate that the temperature of the source rocks and reservoirs never rose over 240 °C (Zou et al., 2014; Zhu et al., 2015; Jiang et al., 2016; Liu et al., 2016, 2018; Yang et al., 2018b). Evidently,

the overall burial temperature was insufficient to form widespread pyrobitumen in both the Ediacaran and Cambrian reservoir of the Chuanzhong Uplift (Yang et al., 2018a; Gao et al., 2018). In addition, the temperature of source rock and reservoirs never rose over 150 °C before the late Permian (Zou et al., 2014; Zhu et al., 2015; Jiang et al., 2016; Liu et al., 2016, 2018; Yang et al., 2018b). Therefore, the maturation of the oil was in moderate level by the time of hydrothermal fluid migration.

The geothermal history has been reconstructed from apatite fission tracks (Liu et al., 2018). Consistency between the simulated and measured reflectance of Vitrinite-like macerals in source rock confirms and supports the reliability of the geothermal history established in previous report by the present authors (Yang et al., 2018a, 2018b; Liu et al., 2018). The powerful hydrothermal fluid invasion could be well correlated to the ELIP during the late Permian, when the heatflow abruptly rose (Liu et al., 2018). The
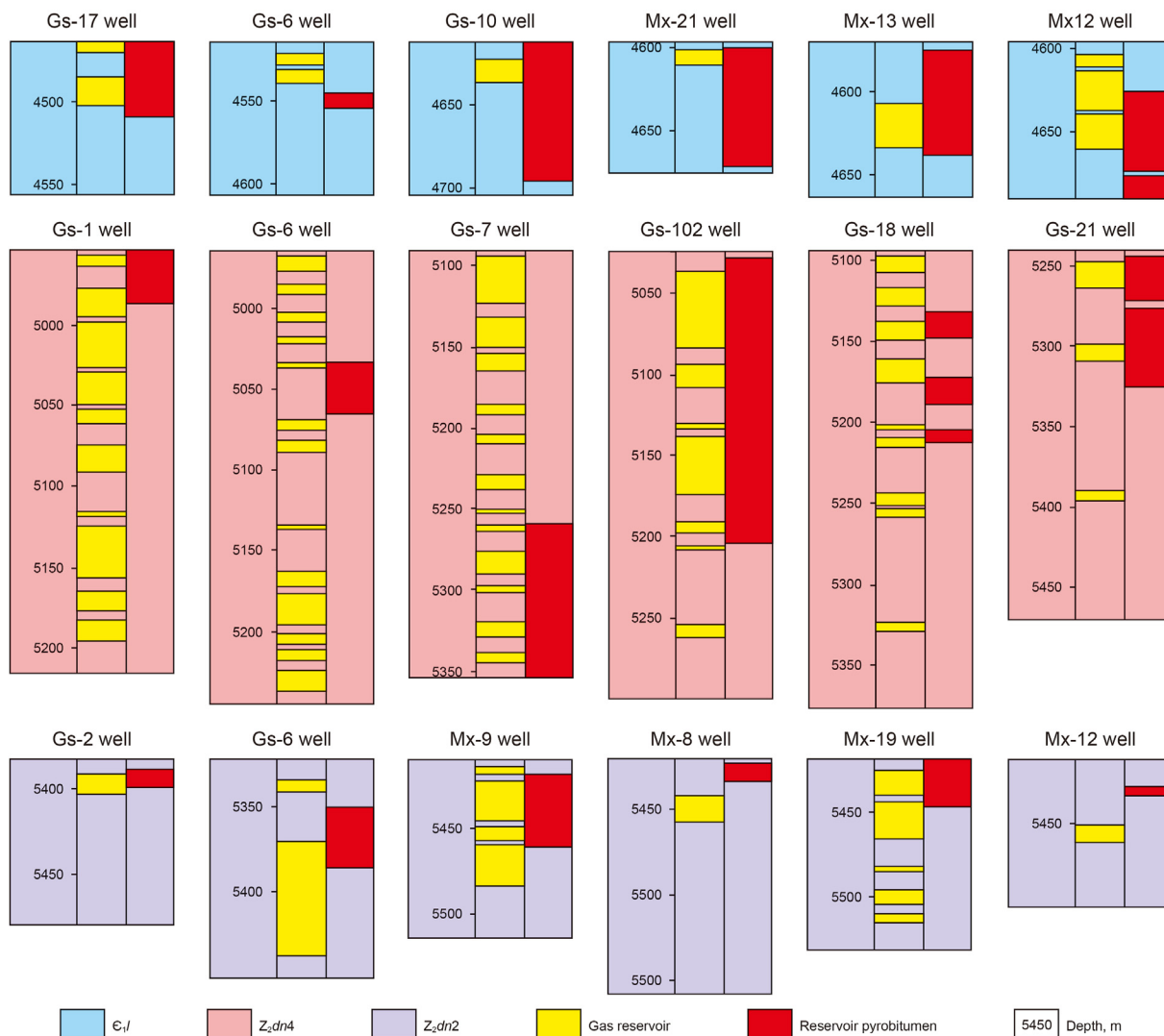
Fig. 5. Distribution of gas reservoir and pyrobitumen in the cored wells.

Table 2
Result of microscopy and elemental analysis of the mesophase and pyrobitumen in the reservoir.

Well	Depth, m	Petrology	H/C	%BR$_{omin}$[a]	%BR$_{omax}$[a]	Mesophase classes occurred in the pyrobitumen	Pyrobitumen classification
Gs-11	4573	dolostone	0.64	3.27	3.32	Mf	MP[b]
Gs-11	4673			0.61	6.30	Mf, Mm, MFA	GP
Mx-12	4659			0.63	6.37	Mf, Mm, Mc, MFA	GP
Mx-204	4663		0.58	0.57	6.55	Mf, SM-Mf, Mm, Mc, MFA, CF	GP
Mx-204	4681			0.46	6.84	Mf, SM-Mf, Mm, Mc, MFA, CF, FD	GP
Gs-17	4968	shale		2.46	2.49	SM-Mf, Mf	MP[b]
Gs-1	4977	dolostone		0.48	6.90	SM-Mf, Mf, Mm, Mc, CF, FD	GP
Gs-2	5013		0.45	0.46	7.74	SM-Mf, Mf, Mm, FD	GP
Mx-9	5033			0.47	7.03	SM-Mf, Mf, Mm, FD	GP
Gs-105	5220		0.4	0.23	8.54	D	DP
Gs-7	5328		0.43	0.37	8.49	D	DP
Mx-51	5395			0.57	7.82	SM-Mm, FD	GP

[a] The %BR$_{omin}$ and %BR$_{omax}$ is the average of top class mesophase in the pyrobitumen sample.
[b] %BR$_{omax}$ of MP is the weighted average of a group of undirected Mfs.

reconstructed heatflow history indicates that there was only one thermal-event during the whole burial process of the reservoir. Therefore, the huge invasion of the hydrothermal fluid should be triggered by a basin scale thermal-event as the ELIP in the late of Permian, which can be apparently exhibited on the heat-flow history curves (Yang et al., 2022).

5.2. Textural evolution of mesophase in pyrobitumen

Persistent polycondensation reactions under high temperatures cause enlargement of condensed macromolecular PAH lamellae which, in turn, has the effect of enhancing the mesophase classes (Lewis and Kovac, 1978; Lewis, 1980, 1987). This is because higher

class mesophase is composed of larger, flatter PAH lamellae, which form more compressed structures (Fig. 2g, i). As previously explained, thermal motion and enlargement of PAH lamellae gradually generates first grain, then flow, and finally domain mesophase (White, 1976; Ragan and Marsh, 1981; Mochida et al., 1984). However, the reservoir pyrobitumen shows the development of three unusual mesophase textures: elliptical grains, orientation of EGs, and multiple classes of mesophase co-occurring in GP.

To date, EG has not been observed in simulation experiments. However all the mesophase grains in the samples in this study are elliptical, which indicates that they were spatially constrained during their early formation from isotropic hydrocarbon liquid during the thermal event (White, 1976; Ragan and Marsh, 1981; Mochida et al., 1984). The only possible explanation for the formation of EG is directional pressure under reservoir conditions.

Santamaria et al. (1999) created mesophase under pressure in the laboratory and found that, at 1 MPa, the rate of coalescence exceeded the rate of growth of the mesophase spheres. As a result, numerous fine mesophase grains in the pitch coalesced to form domain mesophase, while medium and coarse grains were rare. The reason for this phenomenon is viscosity, which is related to pressure. High pressure prevented loss of volatile matter in the pitch, decreasing the viscosity of the coking system, and thus increasing the mobility of the fine grain mesophase (Santamaria et al., 1999). As a result, the small size mesophase spheres preferentially generated more flow and domain mesophase through rapid thermal motion, rather than growing into larger mesophase grains.

Compared to spherical grains, elliptical grains (Fig. 3b and c) in pyrobitumen are easily oriented by thermal motion. The thermal motion firstly orients small EGs, which then coalesce to form flow or domain mesophase. The generation of flow and domain mesophase enhances the viscosity of the pyrobitumen, which temporarily solidifies if the temperature stops increasing, with the result that the multiple classes of mesophase stop evolving and remain together in the GP.

However, the evolution of pyrobitumen is quite different under extremely high temperature-pressure conditions. Goodarzi (1985) reported on the optical properties of vitrinite carbonized at high pressures. Extremely high pressures of 185–310 MPa and high temperatures of over 550 °C downgraded the texture of the mesophase to medium-grained and fine-grained mosaic (Goodarzi, 1985). In addition, numerous micro-vacuoles were observed, dispersed in the mesophase. Interestingly, this honeycomb structure is also observed in the reservoir pyrobitumen (Fig. 6). Apparently, EGs can coalesce and form flow, or even domain mesophase when the %BR_{omax} of the honeycomb structure pyrobitumen reaches 7.82% (Fig. 6b) (Table 2). However, the micro-vacuoles separate the EGs, thereby having the effect of downgrading the mesophase class.

In general, the development of mesophase in reservoir pyrobitumen is affected by both temperature and pressure (Fig. 7). Increasing temperature promotes polycondensation, which enlarges the PAHs and upgrades the mesophase class (Fig. 7). On the other hand, high pressure deforms mesophase spheres into ellipses and orientates the EGs before they coalesce under increasing temperature (Fig. 7). Furthermore, although high pressure reduces the grain sizes in the mesophase (Santamaria et al., 1999), EGs can still coalesce to form flow and domain mesophase if the temperature is sufficiently high (Fig. 7). Therefore, the increasing class of
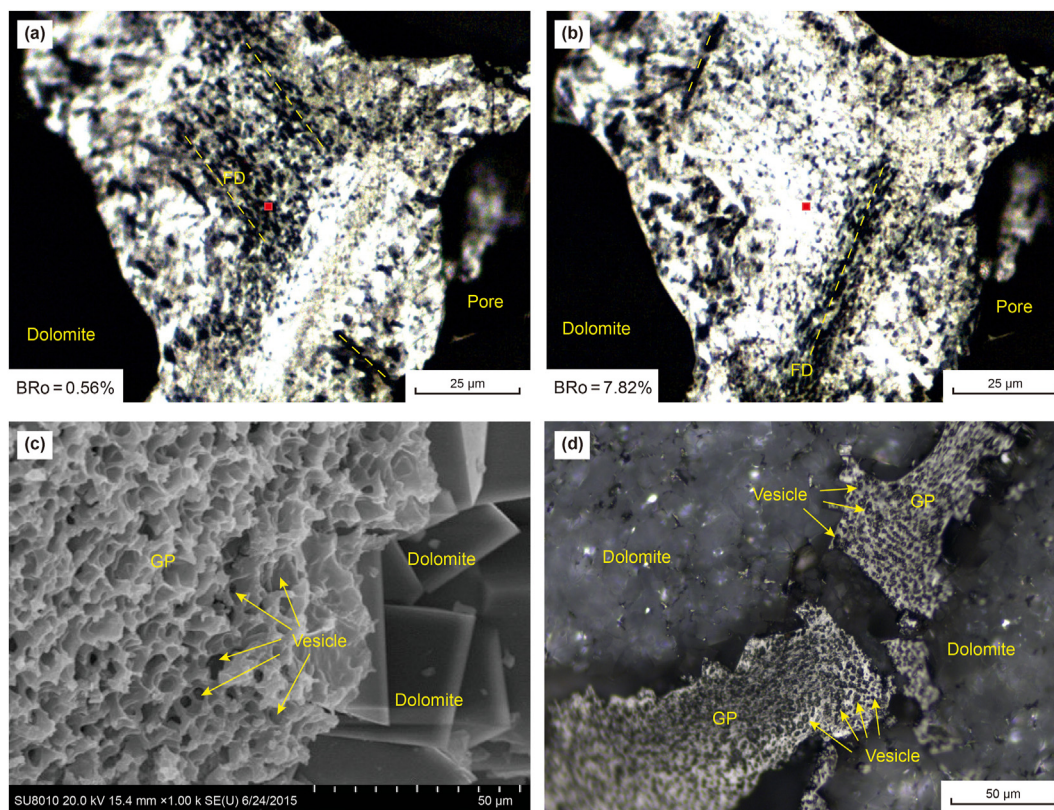

Fig. 6. Optical texture and %BR_o of the SM-Mm mesophase and honeycomb structure in GP in well Mx-51-5935 m. (**a**): texture and %BR_o of the SM-Mm under reflect light; (**b**): texture and %BR_o of the SM-Mm after the rotation of 45° under reflect light; (**c**): the honeycomb structure (SEM); (**d**): the honeycomb structure under reflect light. The red square is the measuring spot which was 1 μm^2.

mesophase in the reservoir pyrobitumen indicates an increasing temperature that the reservoir have ever experienced. Moreover, the elliptical grains, absent of medium class mesophase and honeycomb structure in the pyrobitumen are all the indicators of a high pressure condition.

5.3. Geological temperature and pressure evolution in the reservoir

Under experimental conditions, high temperatures (at least 350 °C) are needed to reduce the viscosity of the pitch during formation of mesophase pyrobitumen (Brooks and Taylor, 1965; White, 1976; Lewis and Kovac, 1978; Forrest and Marsh, 1981). The PAH lamellas in the pitch move rapidly in the high temperature conditions, and the resulting frequent molecular collisions accelerate the formation and textural development of mesophase (Lewis and Kovac, 1978; Lewis, 1980, 1987). However, under geological conditions, reaction times are extended from hours to millions of years (Chung and Jahn, 1995; Liu et al., 2018; Yang et al., 2018b), which means that they are, effectively, unlimited. Development of mesophase therefore requires a relatively high viscosity, because even the molecular collisions of PAH lamellas are very slow, so relatively unlimited time is sufficient to accomplish the reaction.

As a fundamental condition for formation of mesophase, the temperature for a specific mesophase type must never sink below its softening point. As mentioned, higher class mesophase is made from larger size PAH lamellas, which raises the temperature of the softening point, decreases the H/C ratio (Jacob, 1989; Tian, 2013) and increase the %BR$_{omax}$ of the pyrobitumen. The softening point temperature of the highest class mesophase in the pyrobitumen therefore indicates the lowest temperature that it experienced

under geological conditions.

Producing mesophase from coal pitch under experimental conditions indicates that the mesophase H/C ratio (size of PAH lamellas) is negative correlated with its softening point temperature (Tian, 2013). The measured H/C ratio of pyrobitumen in the reservoir is 0.64–0.40 (Table 2). According to the linear relationship between the H/C ratio and the softening point in coal pitch experiments, the softening point temperature for domain mesophase is approximately 200–320 °C (Tian, 2013). Coincidentally, the temperature range of 185–319 °C of the reservoir indicated by the intersection of isochors of methane and coeval aqueous inclusions in quartz (Yang et al., 2018b) is quite close to the softening point of mesophase in pyrobitumen, which is 200–320 °C (Tian, 2013). This softening point range of mesophase is also very close to the statistic data of the softening point range of Grahamite which is 177–316 °C (Jacob, 1989).

Whether the pyrobitumen was generated by coal or oil pitch, the molecular structure of mesophase in the pyrobitumen is similar, especially the high class mesophase (Lewis and Kovac, 1978; Lewis, 1980, 1987). The H/C ratio of pyrobitumen is controlled by the class of the mesophase, thus it may not evidently be affected by the source of the pyrobitumen. During the disproportionation reaction, in post maturity phase, the organic matter have been carbonized. The generation of mesophase indicate the carbonization of organic matter is in final stage because the molecular component and structure of mesophase is fairly close to graphite (Lewis and Kovac, 1978; Lewis, 1980, 1987). Therefore, the different organic matters have a convergent evolution in the disproportionation reaction to form mesophase. This convergent evolution has been reported in the Krevelen's diagram which shows that the H/C of different kinds
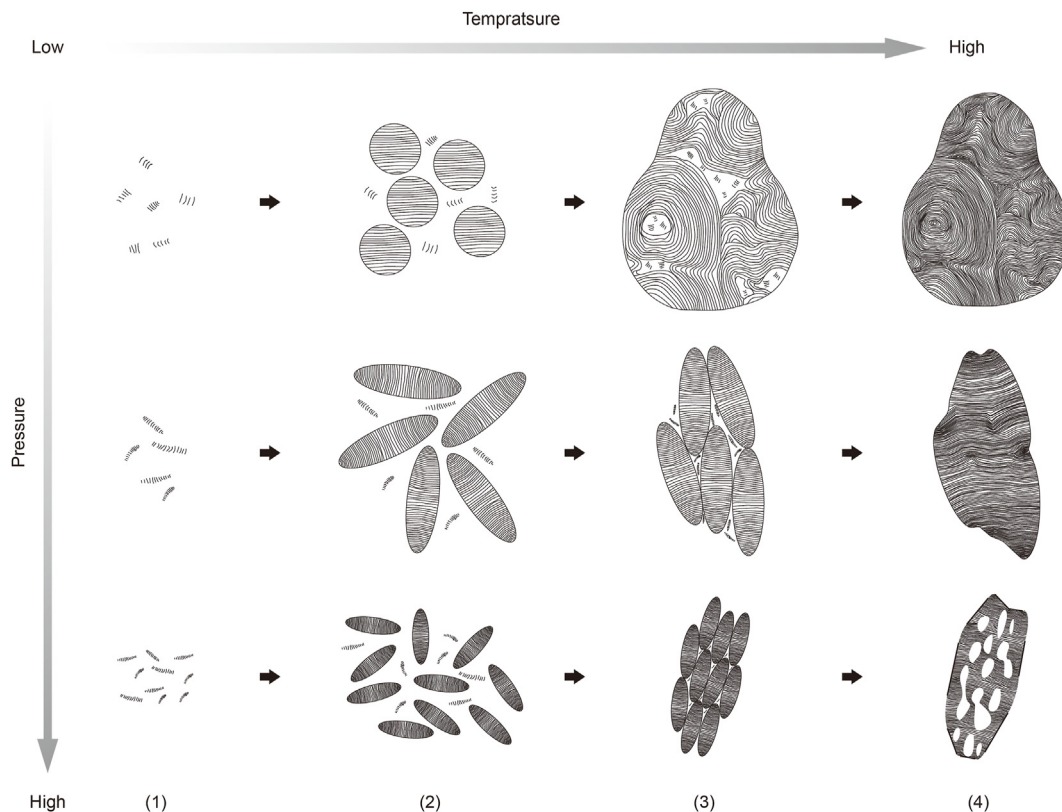

Fig. 7. Schematic diagram of formation and evolution of mesophase in the pyrobitumen.(1) the Mf mesophase were generated and formed the isotropic MP in a relatively low temperature condition, the increasing pressure would press the Mf mesophase into EG; (2) A group of the Mf mesophase coalesced and formed the Mm or Mc, the increasing pressure would decrease the size of the mesophase grain; (3) the higher temperature promoted the coalescence of the mesophase grains, while the increasing pressure led to the orientation at first; (4) the mesophase grains have been coalesced to form flow and domain mesophase, while the extremely high pressure makes a honeycomb structure.
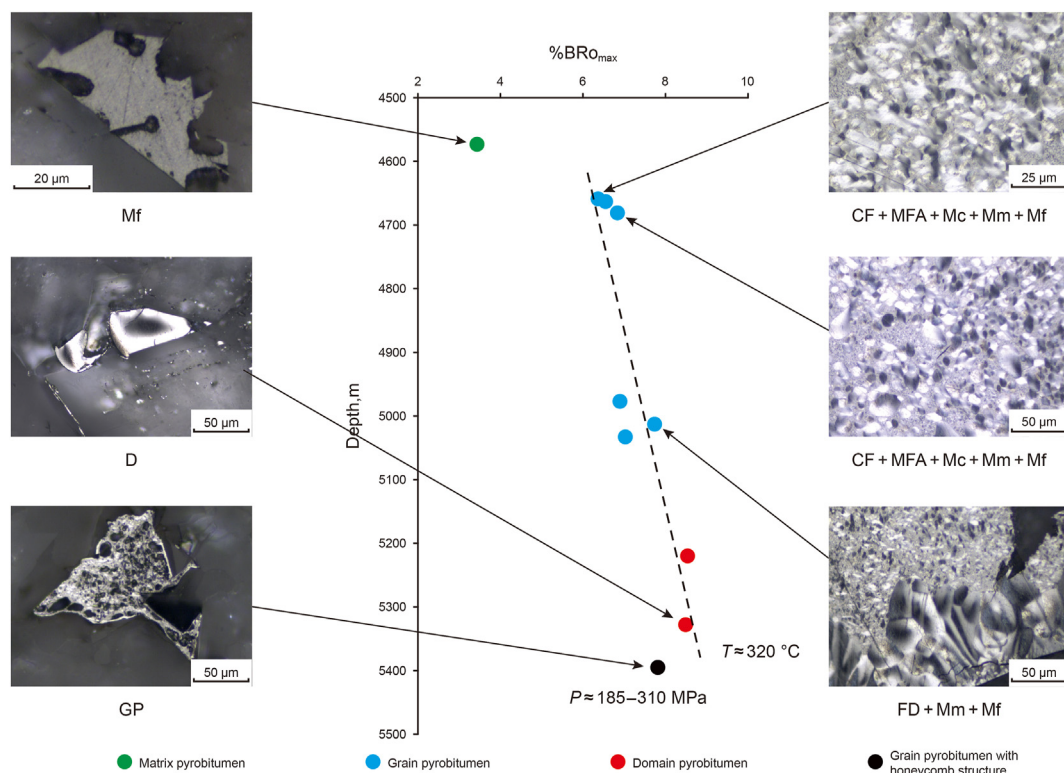
Fig. 8. Optical texture and %BR$_{omax}$ profile of the reservoir in Anyue Gas Felid.

of kerogen have been converged in gas formation stage (Tissot and Welte, 1984). Meanwhile, the oil cracking experiment by Waples have shown that no large or systematic variation in cracking rates or kinetics is apparent for different oil types (Waples, 2000). In any case, the difference of coal and oil pitch in forming pyrobitumen is objectively existing, however the relationship between H/C ratio and the softening point of pyrobitumen from coal pitch could still be a reference for oil coking.

Thermometry of methane inclusions in the gas reservoir of Chuanzhong Uplift identified two sets of temperature-pressure conditions (Yang et al., 2018b). The high temperature-pressure conditions (249–319 °C, 162–230 MPa) may have been created by hydrothermal fluid oil coking and transforming it to pyrobitumen, with the oil coking coevally generating large volumes of gases which significantly increased the pressure in the reservoir (Barker, 1990; Svensen et al., 2009). This thermal event, and the resulting rapid heating, would have caused rapid decomposition of reactive carbon (Svensen et al., 2009), producing gaseous and liquid byproducts which, in the case of the reservoir hydrocarbons, will have further increased the pressure and temperature. The DP in the

Table 3
The present pressure and pressure coefficient of the reservoir in the Anyue Gas Field.

Well	Formation	Measure point depth, m	Measure point pressure, MPa	Pressure coefficient
Mx-8	$\textrm{C}_1l$	4548.9	75.636	1.646
Mx-9		4398.3	75.229	1.693
Mx-11		4597.4	75.769	1.632
Mx-13		4500	75.534	1.662
Mx-202		4500	75.52	1.661
Mx-205		4380	75.13	1.698
Mx-10		4558.8	75.646	1.643
Mx-16		4697.4	76.179	1.606
Mx-17		4492.7	75.526	1.664
Mx-101		4497.1	75.571	1.664
Mx-201		4539.5	75.68	1.65
Mx-21		4559.4	71.83	1.556
Gs-1	Z_2dn4	4744.4	55.8	1.13
Gs-3		4777.9	55.9	1.12
Gs-6		5111	56.65	1.1
Mx-8		4731.9	55.7	1.1
Mx-8	Z_2dn2	4864.3	56.92	1.07
Mx-17		4829.8	57.71	1.1
Gs-1		5217.6	57.25	1.08
Gs-10		5294.7	57.34	1.06

deeper reservoir was generated under a high temperature of approximately 320 °C (Yang et al., 2018b). However, ultra-high pressure of 162−230 MPa (Yang et al., 2018b), analogous to the 185−310 MPa measured in Goodarzi's experiment.

The distribution of pyrobitumen have shown that the oil in the $\textrm{C}_1 l$ reservoir was less heated by the hydrothermal fluid because the mesophase class is relatively lower in the pyrobitumen. Moreover, the class of different mesophase in GP of the $\textrm{C}_1 l$ reservoir is consecutive (Table 2). In addition, some of the grains in these GPs are even spherical (Fig. 2c, f) (Fig. 8). Therefore, the temperature and pressure of $\textrm{C}_1 l$ reservoir was all relatively low while it was heating by the hydrothermal fluid. On the contrary, the class of different mesophase in GP of the $Z_2 dn2$ and $Z_2 dn4$ reservoir is polarized (Table 2). The high class FD and D mesophase occurred together with mostly Mf and Mm mesophase (Fig. 2e, Fig. 8). Moreover, the mesophase grains in the GP of the $Z_2 dn2$ and $Z_2 dn4$ reservoir are all elliptical (Fig. 3). Furthermore, the honeycomb structure discovered only in these deep reservoirs indicates an extremely high pressure which may over 200 MPa (Fig. 8). In sum up, the temperature and pressure of $Z_2 dn2$ and $Z_2 dn4$ reservoirs were evidently higher than that of the $\textrm{C}_1 l$ reservoir while the hydrothermal fluid was heating the paleo-oil field. Nevertheless, the data of present pressure of the reservoir in the Anyue Gas Field shows a totally opposite results (Table 3).

Conversation of the pressure was caused by the gas release after the oil crack in the reservoir (Barker, 1990; Svensen et al., 2009). The generated gases may have gradually dispersed, with the pressure reducing accordingly. After this, relatively low temperature-pressure conditions became established as the pressure system in the reservoir returned to equilibrium (Yang et al., 2018b). The oil crack in $Z_2 dn2$ and $Z_2 dn4$ reservoirs was more thorough because the hydrothermal fluid heating was stronger in the deep formations. The huge overpressure could break the dolostone and release the gases to the upper reservoir or event to the air (Barker, 1990; Svensen et al., 2009). Relatively, the upper $\textrm{C}_1 l$ reservoir was less heated by the hydrothermal fluid. The pressure in this reservoir was increased but insufficient to break the dolostone and to generate a significant decompression. Therefore, the presently measured pressure and pressure coefficient of $\textrm{C}_1 l$ reservoir is all obviously higher than that of the $Z_2 dn2$ and $Z_2 dn4$ reservoirs (Table 3).

6. Conclusions

This study investigates the development of texture and in the Neoproterozoic-Lower Paleozoic dolostone reservoirs in the Chuanzhong Uplift. Even though the geological condition is much more complicated than the experimental condition, mesophase shows a similar evolution regularity in the reservoir and the laboratory.

1. Reservoir pyrobitumen is classified into three types: MP, GP, and DP. MP is composed entirely of Mf mesophase; DP is composed entirely of domain mesophase; and GP is composed of grain, flow, and domain mesophase in varying proportions.
2. The predominant mesophase class in pyrobitumen is controlled by temperature. Pressure deforms mesophase grains into elliptical shapes and orients them before they coalesce to form high class mesophase, while the formation of DP is not significantly affected by pressure.
3. The whole range of MP, GP, and DP indicate a formation temperature between 200−320 °C. However, elliptical grain mesophase, polarized class of mesophase in individual pyrobitumen and honeycomb structure pyrobitumen would be indicators for unusually high formation pressure of the geological conditions during generation of the pyrobitumen.

4. Gases in the Anyue Gas Field was generated by the hydrothermal fluid heating of the paleo oil. The oil crack in the $Z_2 dn2$ and $Z_2 dn4$ reservoir was stronger than that in the $\textrm{C}_1 l$ reservoir. Calculating by the intersection of isochors of methane and coeval aqueous inclusions in quartz indicates that the oil crack therefore created an extremely high pressure in the $Z_2 dn2$ and $Z_2 dn4$ reservoir up to over 200 MPa which would break the dolostone and release the gases. Subsequently, the pressure in the reservoir have been converted at present.

References

Barker, C., 1990. Calculated volume and pressure changes during the cracking of oil and gas in reservoirs. AAPG (Am. Assoc. Pet. Geol.) Bull. 74 (8), 1254−1261. https://doi.org/10.1306/0C9B247F-1710-11D7-8645000102C1865D.

Basuki, N.I., Spooner, E.T.C., 2004. A review of fluid inclusion temperatures and salinities n Mississippi Valley-type Zn-Pb deposits: identifying thresholds for metal transport. Explor. Min. Geol. 11, 1−17. https://doi.org/10.2113/11.1-4.1.

Brooks, J.D., Taylor, G.H., 1965. Formation of graphitizing carbons from the liquid phase. Nature 3, 697−699. https://doi.org/10.1016/0008-6223(65)90047-3.

Chung, S.L., Jahn, B., 1995. Plume-lithosphere interaction in generation of the Emeishan flood basalts at the Permian-Triassic boundary. Geology 23, 889 https://doi.org/0.1130/0091-7613(1995)023<0889:PLIIGO>2.3.CO;2.

Emmanuel, S., Eliyahu, M., Day-Stirrat, R.J., Hofmann, R., 2016. Impact of thermal maturation on nano-scale elastic properties of organic matter in shales. Mar. Petrol. Geol. 70, 175−184. https://doi.org/10.1016/j.marpetgeo.2015.12.001.

Forrest, M., Marsh, H., 1981. Composition of pore-wall material in metal-lurgical coke: considerations of strength, gasification and thermal stress. Fuel 60, 418−422. https://doi.org/10.1016/0016-2361(81)90280-5.

Gao, P., Liu, G., Lash, G.G., Li, B., Yan, D., Chen, C., 2018. Occurrences and origin of reservoir solid bitumen in Sinian Dengying formation dolomites of the Sichuan basin, SW China. Int. J. Coal Geol. 200, 135−152. https://doi.org/10.1016/j.coal.2018.11.001.

Gentzis, T., Goodarzi, F., 1993. Maturity studies and source-rock potential in the southern Sverdrup Basin, Arctic Canada. Int. J. Coal Geol. 24 (1−4), 141−177. https://doi.org/10.1016/0166-5162(93)90008-X.

Goodarzi, F., 1984. Optical properties of high-temperature heat-treated vitrinites. Fuel 63 (6), 820−826. https://doi.org/10.1016/0016-2361(84)90074-7.

Goodarzi, F., 1985. Optical properties of vitrinite carbonized under pressure. Fuel 64, 158−162. https://doi.org/10.1016/0016-2361(85)90209-1.

Goodarzi, F., Stasiuk, L.D., 1991. Thermal alteration of Gilsonite due to bushfire, an example from southwest Iran. Inter. Int. J. Coal Geol. 17 (3−4), 333−342. https://doi.org/10.1016/0166-5162(91)90038-K.

Greinke, R.A., 1990. Quantitative influence of dealkylation and polymerization reactions on mesophase formation. Carbon 28 (5), 701−706. https://doi.org/10.1016/0008-6223(90)90072-7.

Hackley, P.C., Cardott, B.J., 2016. Application of organic petrography in North America shale petroleum systems: a review. Int. J. Coal Geol. 163, 8−51. https://doi.org/10.1016/j.coal.2016.06.010.

He, B., Xu, Y.G., S-L, C., Xiao, L., Wang, Y., 2003. Sedimentary evidence for a rapid, kilometer-scale crustal doming prior to the eruption of the Emeishan flood basalts. Earth Planet Sci. Lett. 213, 391−405. https://doi.org/10.1016/S0012-821X(03)00323-6.

Jacob, H., 1989. Classification, structure, genesis and practical importance of natural solid oil bitumen ("migrabitumen"). Int. J. Coal Geol. 11, 65−79. https://doi.org/10.1016/0166-5162(89)90113-4.

Jiang, Y., Tao, Y., Gu, Y., Wang, J., Guang, Z., Jiang, N., Lin, G., Jiang, C., 2016. Hydrothermal dolomitization in Dengying formation, gaoshiti-moxi area, Sichuan Basin, SW China. Petrol. Explor. Dev. 43, 54−64. https://doi.org/10.1016/S1876-3804(16)30006-4.

Klett, J., Hardy, R., Romine, E., Walls, C., Burchell, T., 2000. High-thermal-conductivity, mesophase-pitch-derived carbon foams: effect of precursor on structure and properties. Carbon 38, 953−973. https://doi.org/10.1016/S0008-6223(99)00190-6.

Kilby, W.E., 1988. Recognition of vitrinite with non-uniaxial negative reflectance characteristics. Int. J. Coal Geol. 9, 267−285. https://doi.org/10.1016/0166-5162(88)90017-1.

Large, R.R., Bull, S.W., Selley, D., Yang, J., Mcgoldrick, P.J., 2002. Controls on the formation of giant stratiform sediment-hosted Zn-Pb-Ag deposits: with

particular reference to the north Australian Proterozoic. In: Giant Ore Deposits: Characteristics, Genesis and Exploration, ISBN 1-86295-040-7 (Refereed Conference Paper).

Leach, D.L., Bradley, D.C., Huston, D., Pisarevsky, S.A., Taylor, R.D., Gardoll, T.J., 2010. Sediment-hosted lead-zinc-deposits in earth history. Econ. Geol. 105 (3), 593–625. https://doi.org/10.2113/gsecongeo.105.3.593.

Leach, D.L., Sangster, D.F., Kelley, K.D., Large, R.R., Garven, G., Allen, C.R., Gutzmer, J., Walters, S., 2005. Sediment-hosted lead-zinc deposits-a global perspective. Econ. Geol. 100, 561–607. https://doi.org/10.1016/0008-6223(78)90100-8.

Lewis, I.C., 1978. Thermotropic mesophase pitch. Carbon 16 (6), 503. https://doi.org/10.1016/0008-6223(78)90100-8.

Lewis, I.C., 1980. Thermal polymerization of aromatic hydrocarbons. Carbon 18, 191–196. https://doi.org/10.1016/0008-6223(80)90060-3.

Lewis, I.C., 1987. Chemistry of pitch carbonization. Fuel 66 (11), 1527–1531. https://doi.org/10.1016/0016-2361(87)90012-3.

Lewis, I.C., Kovac, C.A., 1978. The role of free radicals and molecular size in mesophase pitch. Carbon 16 (6), 425–429. https://doi.org/10.1016/0008-6223(78)90087-8.

Liu, Q., Zhu, D., Jin, Z., Liu, C., Zhang, D., He, Z., 2016. Coupled alteration of hydrothermal fluids and thermal sulfate reduction (TSR) in ancient dolomite reservoirs − an example from Sinian Dengying Formation in Sichuan Basin, southern China. Precambrian Res. 285, 39–57. https://doi.org/10.1016/j.precamres.2016.09.006.

Liu, W., Qiu, N., Xu, Q., Liu, Y., 2018. Precambrian temperature and pressure system of Gaoshiti-Moxi block in the central paleo-uplift of Sichuan Basin, southwest China. Precambrian Res. 313, 91–108. https://doi.org/10.1016/j.precamres.2018.05.028.

Luo, Q., Zhong, N., Qin, J., Li, K., Zhang, Y., Wang, Y., Ma, Ling, 2014. Thucholite in Mesoproterozoic shales from northern north China: occurrence and indication for thermal maturity. Int. J. Coal Geol. 125, 1–9. https://doi.org/10.1016/j.coal.2014.01.009.

Luo, Q., Hao, J., Skovsted, C.B., Luo, P., Khan, I., Wu, J., Zhong, N., 2017. The organic petrology of graptolites and maturity assessment of the Wufeng−Longmaxi formations from Chongqing, China: insights from reflectance cross-plot analysis. Int. J. Coal Geol. 183, 161–173. https://doi.org/10.1016/j.coal.2017.09.006.

Marsh, H., 1973. Carbonization and liquid-crystal (mesophase) development: Part 1. The significance of the mesophase during carbonization of coking coals. Fuel 52, 205–212. https://doi.org/10.1016/0016-2361(73)90080-X.

Mastalerz, M., Agnieszka, D., Stankiewicz, A.B., 2018. Origin, properties, and implications of solid bitumen in source-rock reservoirs: a review. Int. J. Coal Geol. 195, 14–36. https://doi.org/10.1016/j.coal.2018.05.013.

Mochida, I., Korai, Y., Fujitsu, H., Takeshita, K., Komatsubara, Y., Koba, K.I., Marsh, H., 1984. Aspects of gasification and structure in cokes from coals. Fuel 63, 136–139. https://doi.org/10.1016/0016-2361(84)90270-9.

Ragan, S., Marsh, H., 1981. Carbonization and liquid-crystal (mesophase) development. 22. Micro-strength and optical textures of cokes from coal-pitch cocarbonizations. Fuel 60 (6), 522–528. https://doi.org/10.1016/0016-2361(81)90116-2.

Rimmer, S.M., Crelling, J.C., Yoksoulian, L.E., 2015. An occurrence of coked bitumen, Raton Formation, Purgatoire River Valley, Colorado, U.S.A. Int. J. Coal Geol. 141–142, 63–73. https://doi.org/10.1016/j.coal.2015.02.010.

Rippen, D., Littke, R., Bruns, B., Mahlstedt, N., 2013. Organic geochemistry and petrography of Lower Cretaceous Wealden black shales of the Lower Saxony Basin: the transition from lacustrine oil shales to gas shales. Org. Geochem. 63, 18–36. https://doi.org/10.1016/j.orggeochem.2013.07.013.

Santamaria, R.R., Romero, P.E., Gomez, S.C., Rodrıguez, R., Martınez, S.S., Martınez, M., Mar, H., 1999. Influence of pressure variations on the formation and development of mesophase in a petroleum residue. Carbon 37, 445–455. https://doi.org/10.1016/S0008-6223(98)00211-5.

Stach, E., Mackowsky, M.T., Teichmüller, M., Taylor, G.H., Chandra, D., Teichmüller, R., 1982. Textbook of Coal Petrology. Gebrüder Borntraeger, Berlin, Stuttgart.

Stasiuk, L.D., 1997. The origin of pyrobitumens in upper Devonian Leduc formation gas reservoirs, Alberta, Canada: an optical and EDS study of oil to gas transformation. Mar. Petrol. Geol. 14, 915–929. https://doi.org/10.1016/S0264-8172(97)00031-7.

Svensen, H., Planke, S., Polozov, A.G., Schmidbauer, N., Corfu, F., Podladchikov, Y.Y., Jamtveit, B., 2009. Siberian gas venting and the end-Permian environmental crisis. Earth Planet Sci. Lett. 277, 490–500. https://doi.org/10.1016/j.epsl.2008.11.015.

Tian, Y.J., 2013. Source Material Separation of Mesophase Spherule and Preparation and Application of Carbonaceous Mesophase (Doctoral dissertation).

Tissot, B.P., Welte, D.H., 1984. Petroleum Formation and Occurrence. Springer-Verlag. https://doi.org/10.1007/978-3-642-87813-8.

Wang, M.Z., 1990. Liquid-Phase Carbonization of Organic Compounds, 012 Chinese Chem. Soc. (44), 22–28. https://doi.org/10.14159/j.cnki.0441-3776.1990.12.004.

Waples, D.W., 2000. The kinetics of in-reservoir oil destruction and gas formation: constraints from experimental and empirical data, and from thermodynamics. Org. Geochem. 31, 553–575. https://doi.org/10.1016/S0146-6380(00)00023-1.

Wei, G., Shen, P., Yang, W., Zhang, J., Jiao, G., Xie, W., Xie, Z., 2013. Formation conditions and exploration prospects of Sinian large gas fields, Sichuan Basin. Petrol. Explor. Dev. 40, 139–149. https://doi.org/10.1016/S1876-3804(13)60017-8.

White, J.L., 1976. Mesophase Mechanisms in the Formation of the Microstructure of Petroleum Coke. Am. Chem. Soc. Division of Petrol. Chem., Preprints 29 (2), 388–397.

Yang, C., Ni, Z., Li, M., Wang, T., Chen, Z., Hong, H., Tian, X., 2018a. Pyrobitumen in South China: Pyrobitumen, chemical composition and geological significance. Int. J. Coal Geol. 188, 51–63. https://doi.org/10.1016/j.coal.2018.01.014.

Yang, C., Ni, Z., Wang, T., Chen, Z., Hong, H., Wen, L., Luo, B., Wang, W., 2018b. A new genetic mechanism of natural gas accumulation. Sci. Rep. 8, 8336. https://doi.org/10.1038/s41598-018-26517-y.

Yang, C., Li, M., Ni, Z., Wang, T., Qiu, N., Fang, R., Wen, L., 2022. Paleo-oil reservoir pyrolysis and gas release in the Yangtze Block imply an alternative mechanism for the Late Permian Crisis. Geosci. Front. 13 (2), 14. https://doi.org/10.1016/j.gsf.2021.101324.

Zhu, G., Wang, T., Xie, Z., Xie, B., Liu, K., 2015. Giant gas discovery in the Precambrian deeply buried reservoirs in the Sichuan Basin, China: Implications for gas exploration in old cratonic basins. Precambrian Res. 262, 45–66. https://doi.org/10.1016/j.precamres.2015.02.023.

Zou, C., Jinhu, D.U., Chunchun, X.U., Wang, Z., Zhang, B., Wei, G., Wang, T., Yao, G., Deng, S., Liu, J., 2014. Formation, distribution, resource potential, and discovery of Sinian−Cambrian giant gas field, Sichuan Basin, SW China. Petrol. Explor. Dev. 41 (3), 306–325. https://doi.org/10.1016/S1876-3804(14)60036-7.